G_2/M cell cycle arrest on HT-29 cancer cells and toxicity assessment of triphenylphosphanegold(I) carbonimidothioates, $Ph_3PAu[SC(OR) = NPh]$, R = Me, Et, and iPr, during zebrafish development

Kah Kooi Ooi [a,b], Chien Ing Yeo [b], Theventhiran Mahandaran [c], Kok Pian Ang [a], Abdah Md Akim [a], Yoke-Kqueen Cheah [a], Hoi-Ling Seng [d,*], Edward R. T. Tiekink [b,**]

[a] *Department of Biomedical Science, Faculty of Medicine and Health Sciences, University Putra Malaysia, 43400 UPM Serdang, Selangor, Malaysia*

[b] *Research Centre for Crystalline Materials, Faculty of Science and Technology, Sunway University, 47500 Bandar Sunway, Selangor Darul Ehsan, Malaysia*

[c] *Department of Biotechnology, Faculty of Engineering and Science, Malaysia University of Science and Technology, 47301 Petaling Jaya, Selangor, Malaysia*

[d] *Department of Biological Sciences, Faculty of Science and Technology, Sunway University, 47500 Bandar Sunway, Selangor Darul Ehsan, Malaysia*

* Corresponding author: Tel.: +60 3 7491 7168; fax: +60 3 7491 8633

** Corresponding author: Tel.: +60 3 7491 7173; fax: +60 3 7491 8633

E-mail addresses: hoilings@sunway.edu.my (H.-L. Seng), edwardt@sunway@edu.my (E.R.T. Tiekink)

ABSTRACT

Phosphanegold(I) thiolates, $Ph_3PAu[SC(OR) = NPh]$, R = Me (**1**), Et (**2**) and iPr (**3**), were previously shown to be significantly cytotoxic toward HT-29 cancer cells and to induce cell death by both intrinsic and extrinsic apoptotic pathways whereby **1** activated the p73 gene, and each of **2** and **3** activated p53; **2** also caused apoptotic cell death via the c-Jun N-terminal kinase/mitogen-activated protein kinase pathway. Apoptosis pathways have been further evaluated by mitochondrial cytochrome c measurements and annexin V screening, confirming apoptotic pathways of cell death. Cell cycle analysis showed the majority of treated HT-29 cells were arrested at the G_2/M checkpoint after 24 h; results of both assays were confirmed by changes in populations of relevant genes (PCR array analysis). Cell invasion studies showed inhibition of metastasis through Matrigel™ matrix to 17-22 % cf. untreated cells. LC_{50} values were determined in zebrafish (8.36, 8.17, and 7.64 μM for **1**–**3**). Finally, the zebrafish tolerated doses of **1** and **2** up to 0.625 μM, and **3** was tolerated at even higher doses of up to 1.25 μM.

Abbreviations

Annexin V-FITC	Recombinant annexin V conjugated to fluorescein isothiocyanate
APAF-1	Apoptotic protease activating factor 1
ATR	Ataxia telangiectasia and Rad3-related
Bax	Apoptosis regulator
Bcl-2	B-cell lymphoma 2
BIRC-5	Baculoviral inhibitor of apoptosis repeat-containing 5/ Survivin
CCNB1	Cyclin B1
cdc25C	Cell division cycle 25C

CDKN1A	Cyclin-dependent kinase N1A
CDK2	Cyclin-dependent kinase 2
CDK4	Cyclin-dependent kinase 4
CHEK1/Chk1	Checkpoint kinase 1
CHEK2/Chk2	Checkpoint kinase 2
c-Src	Proto-oncogene tyrosine-protein kinase
dpf	day(s) post fertilization
FAK	Focal adhesion kinase
FSC	Forward scatter
GADD45	Growth arrest DNA-damage-inducible protein 45
G_1 Phase	Gap-1 Phase
G_2 Phase	Gap-2 Phase/Pre-mitotic phase
G_2/M Phase	Gap-2/Mitotic Phase
hpf	hour(s) post fertilization
JNK	c-Jun N-terminal kinase
LC_{50}	lethal concentration required to kill 50% of the population
M Phase	Mitotic phase
MAPK	Mitogen-activated protein kinase
MMP2	Matrix metalloproteinase-2
MMP9	Matrix metalloproteinases-9
NF-κB	Nuclear Factor Kappa Beta
PBS	Phosphate buffered saline
PCR	Polymerase chain reaction

PI	Propidium iodide
PS	Phosphatidylserine
p21	Potent cyclin-dependent kinase inhibitor
p53	Tumor suppressor gene p53
p73	Tumor suppressor gene p73
ROS	Reactive oxygen species
S Phase	Synthesis phase
SSC	Side scatter
Tcf	T-cell factor
XIAP	X chromosome-linked IAP

Keywords: Gold(I) compounds; carbonimidothioates; phosphanegold(I) thiolates; apoptosis; HT-29 cancer cell; zebrafish

1. Introduction

Phosphanegold(I) compounds showed early promise as anticancer drugs through biological screening [1-8] and evaluation of mechanistic pathways [3-8]. For example, in recent years evidence has accumulated suggesting phosphanegold(I) compounds are responsible for mitochondrial dysfunction leading to cell death [3-8]. The importance of mitochondria as useful targets in cancer cells arises because they serve as a reservoir of proteins that stimulate the apoptotic death when mobilized into the cytosol [9,10]. Moreover, mitochondria employ both vital and lethal functions in physiological and pathological conditions.

In the cell cycle checkpoint signaling cascade, mediators provide a platform for signal transduction, activated transducers, DNA damage sensors, and their effectors leading to cell cycle arrest and other necessary metabolic actions [11]. Eukaryotic cell cycle checkpoints are responsible for the regulation of sequential formation, activation, and subsequent inactivation of cyclin dependent kinases, the activation of which is dependent upon an association with cyclins [12]. Therefore, failing to maintain genomic integrity results in accretion of multiple deleterious mutations and may lead to cancer development [11]. Furthermore, deregulation of the cell cycle resulting in uncontrolled cell proliferation, is one of the most common alterations that occurs during tumor development [13]. Consequently, the blockage of the cell cycle is regarded as an important operative strategy for killing cancer cells [14].

The use of zebrafish (*Danio rerio*) has emerged as a powerful model system to monitor angiogenesis *in vivo* [15-17]. Zebrafish have been used as a model organism for research purposes for more than 20 years and therefore handling methods, optimum breeding techniques, husbandry, and maintenance are well established [18]. Recent research has shown that most of the genes found in humans have at least one zebrafish orthologue [19]. The above ensures zebrafish as being highly useful for the study of complex biological processes such as cell

senescence and apoptosis, aging, cardiovascular system development, and drug toxicity response [15-21]. There are a few special characteristics of zebrafish that are worth highlighting. In particular, the transparency of zebrafish embryos is of great advantage as this allows real time assessment of organogenesis and phenotypic changes during both drug and toxicity trials [20]. Zebrafish embryos can absorb drugs *ex vivo* through their egg membrane or skin [21] thereby adding to their utility for drug evaluation. This aspect has the considerable advantage of making it possible to treat an embryo with a drug and then to observe real time changes by simply employing a microscope.

It was recently reported that $Ph_3PAu[SC(OR) = NPh]$, R = Me (**1**), Et (**2**) and iPr (**3**), exhibited significant cytotoxicity to the HT-29 cancer cell line and induced both intrinsic and extrinsic apoptotic pathways [22]. Specifically, it was demonstrated that **1** activates the p73 gene in contrast to each of **2** and **3** which activate the p53 gene. Further, an additional apoptotic mechanism was induced by **2**, namely via the JNK/MAP pathway [22]. Given these promising early results, the present work continues an investigation of **1**–**3** by delving more deeply into cell apoptosis, release of cytochrome c, cell invasion, cell cycle analysis, gene expression, and *in vivo* toxicity assessment during zebrafish development.

2. Experimental

2.1 Instrumentation for chemical analysis

Elemental analyses were performed on a Perkin Elmer PE 2400 CHN Elemental Analyser. ^{1}H and $^{13}C\{^{1}H\}$ NMR spectra were recorded in $CDCl_3$ solutions on a Bruker Avance 400 MHz NMR spectrometer with chemical shifts relative to tetramethylsilane. $^{31}P\{^{1}H\}$ NMR spectra were recorded in $CDCl_3$ solution on the same instrument with the chemical shifts recorded relative to 85% aqueous H_3PO_4 as the external reference. Stock solutions of $Ph_3PAu\{SC(OR) = NC_6H_5\}$, for R = Me, Et and iPr, were prepared in acetonitrile for the photoluminescence (1

x 10^{-3} M) and UV (1 x 10^{-5} M) measurements. The optical absorption spectra were measured in the range 190–1100 nm on a single-beam Agilent Cary 60 UV-Vis spectrophotometer. Photoluminescence (PL) measurements were carried out on an Agilent Varian Cary Eclipse Fluorescence Spectrophotometer using a Xenon flash lamp as the excitation source at room temperature.

2.2 Synthesis

All reactions were carried out under ambient conditions. All chemicals and solvents were sourced commercially and used as received. The thiocarbamides and triphenylphosphanegold(I) complexes were prepared as described previously [22].

*2.2.1 $Ph_3PAu[SC(OMe) = NC_6H_5]$ **(1)***

Anal. Calc. for $C_{26}H_{23}AuNOPS$: C, 49.93; H, 3.71; N, 2.24. Found: C, 49.69; H, 3.45; N, 2.28. UV (acetonitrile, 1.0 x 10^{-5} M): λ_{max} = 240 nm (ε = 2.3 x 10^3 cm^{-1} M^{-1}); 267 (1.2 x 10^3); 275 (1.1 x 10^3) nm. PL (acetonitrile, 1 x 10^{-3} M, λ_{ex} = 240 nm): 336, 422, 488, 533 (sh), 582 (sh) nm.

*2.2.2 $Ph_3PAu[SC(OEt) = NC_6H_5]$ **(2)***

Anal. Calc. for $C_{27}H_{25}AuNOPS$: C, 50.71; H, 3.94; N, 2.19. Found: C, 50.64; H, 3.75; N, 2.26. UV (acetonitrile, 1.0 x 10^{-5} M): λ_{max} = 240 nm (ε = 2.5 x 10^3 cm^{-1} M^{-1}); 267 (1.2 x 10^3); 275 (1.0 x 10^3) nm. PL (acetonitrile, 1 x 10^{-3} M, λ_{ex} = 240 nm): 336, 422, 488, 532 (sh), 590 (sh) nm.

*2.2.3 $Ph_3PAu[SC(OiPr) = NC_6H_5]$ **(3)***

Anal. Calc. for $C_{28}H_{27}AuNOPS$: C, 51.46; H, 4.16; N, 2.14. Found: C, 51.31; H, 3.84; N, 2.39. UV (acetonitrile, 1.0 x 10^{-5} M): λ_{max} = 240 nm (ε = 2.6 x 10^3 cm^{-1} M^{-1}); 267 (1.2 x 10^3);

275 (1.0 x 10^3) nm. PL (acetonitrile, 1 x 10^{-3} M, λ_{ex} = 240 nm): 336, 422, 488, 533 (sh), 582 (sh) nm.

2.3 Mitochondrial cytochrome c measurements

The HT-29 cells were cultured at a density of 1 x 10^6 cells/mL. The cells were treated with the previously determined IC_{50} concentrations of **1**–**3**, i.e., 11.30, 17.20, and 16.80 µM, respectively [22], and incubated at 37 ºC for 6, 12, and 24 h. After harvesting, the cells were permeabilized, stained, and fixed according to the standard protocols (FlowCellet™ Cytochrome C Kit, Millipore, Germany). The samples were then analyzed using a flow cytometer (FASCalibur™, BD Biosciences) equipped with BD cell-fit software™; the band pass filter for anti-cytochrome c-FITC is 488 nm. Each of the forward scatter (FSC) and side scatter (SSC) was slightly adjusted to exclude debris and cell aggregates. The experiments were performed in duplicate.

2.4 Flow cytometry for cell apoptosis analysis

Cells were cultured to a density of 1 x 10^6 cells/mL and treated with the IC_{50} concentrations of each compound, and incubated for 6 and 24 h. 1 % DMSO was the negative control. After induction of apoptosis the cells were harvested and washed with ice cold PBS twice, and then resuspended in 500 µL of ice cold 1X binding buffer. The treatment groups were stained with Annexin V-FITC and propidium iodide (PI) according to the manufacturer's protocols (ApopNexin™ FITC Apoptosis Detection Kit, Chemicon, Canada). The suspension was then incubated for 20 min at room temperature in the absence of light. Calibration of the flow cytometer (FACSCalibur™, BD Biosciences) was required to allow for electronic compensation and to determine quadrant statistics. The cells were then sent for bi-color analysis (band pass filter for FITC is 530 nm and is 600 nm for PI). Each of the FSC and SSC

was slightly adjusted to exclude debris and cell aggregates. The experiments were performed in duplicate.

2.5 Flow cytometry for cell cycle analysis

The wells were seeded with 3 x 10^5 cells/mL, treated with IC_{50} doses of **1**–**3**, and incubated for 6, 12, and 24 h. The cells were collected after the specified incubation time and after washing twice with ice cold PBS, were fixed in ice cold 70 % ethanol, and then stored overnight at -20 ^oC. Prior to cell cycle analysis each sample was washed again with ice cold PBS to remove excess ethanol and to rehydrate the cells. PBS was added to resuspend the cell pellet, RNase A (1 mg/mL) and PI (1 mg/mL) were added followed by incubation for 30 min at room temperature in the dark, and placed on ice before analysis on a flow cytometer (FASCalibur™, BD Biosciences). The PI fluorescence was measured at 488 nm laser illumination. The number of events at each of the stages of cell cycle was expressed as a percentage. The experiments were performed in duplicate.

2.6 Extraction of RNA, and RT^2 Profiler PCR microarray (cell cycle analysis)

The cells were plated at a density of 3 x 10^6 cells per T-75 cm^2 flask. Total RNA was extracted from the cultured HT-29 cells using a high purity RNeasy Mini Kit (Qiagen, USA) according to the manufacturer's protocol. Total RNA samples were dissolved in diethylpyrocarbonate treated water and their concentration and quality were analyzed by electrophoresis and UV-vis spectroscopy (BioPhotometer Spectrophotometer UV/VIS, Eppendorf, Germany).

The real-time PCR for microarray assay was performed using the RT^2 Profiler PCR microarray cell cycle (PHAS-020) according to the manufacturer's protocol (Qiagen, Germany). The Human Cell Cycle RT^2 Profiler™ PCR Array profiles the expression of 84

genes key to cell cycle regulation. This array contains genes that both positively and negatively regulate the cell cycle, the transitions between the each of the phases, DNA replication, checkpoints, and arrest. Gene expression was compared according to the threshold cycle (Ct) value. The experiments were performed in duplicate.

2.7 Cell invasion assay

The wells were prepared with a concentration of 5 x 10^4 cells/mL. The experiment was performed by following the protocols of the BD Biosciences (San Jose, CA) Matrigel™ Invasion Chamber. The cells were treated with the IC_{50} doses of **1**–**3** and incubated for 24 h. Non invading cells were removed from the upper surface of the membrane by gently scrubbing with a cotton tipped swab. The inserts were then stained. The cells were fixed with absolute methanol for 2 min, followed by staining with 1 % toluidine blue O (Sigma-Aldrich), and washed with PBS. The insert was placed on a glass slide and observed under a light microscope with 200x magnification (Ziess, USA). Cell counting was facilitated by photographing the membrane and by direct counting with the aid of cell counter. Data were measured in triplicate and are shown as mean ± SEM; SEM = standard error of the mean.

2.8 Zebrafish culture and embryo selection

Adult zebrafish (*Danio rerio*) were obtained from the Faculty of Science and Technology, University of Malaysia Terengganu (Terengganu, Malaysia). Fish were fed with commercially available fish food twice daily and kept at approximately 28 ºC with a 14/10 h light/dark photoperiod in a flow through system. Plastic embryo collection traps were set between 4 and 6 pm and collected the following morning within 1 h of spawning between 9 and 10 am. Collected embryos were placed in petri dishes containing egg water and incubated at 28 ºC until separated into experimental groups. The spawning finished at the beginning of the light

cycle and the fertilized eggs were washed twice with fish culture medium. The embryos were collected 2 h post fertilization (hpf) and examined under a stereomicroscope. Embryos that had developed normally and reached the blastula stage were selected for subsequent experiments.

2.9 Embryo testing

First, 40 embryos were placed in 48-well plates (one embryo/well) and at 2 hpf exposed to different concentrations of compounds **1**–**3** (0.625-10.0 µM) in 0.1 % DMSO incubated in E3 medium (0.3 g NaCl, 0.013 g KCl, 0.05 g $CaCl_2$, 0.08 g $MgSO_4$, and 0.05 % methylene blue) at 28 ºC. As a negative control 0.1 % DMSO treated embryos were used. Exposures were carried out in duplicate (two plates). All larvae were screened daily under a microscope and were examined until 3 days post fertilization (dpf). The procedure was performed in the dark. Digital images of embryos and larvae in lateral orientations were taken every day under a stereomicroscope at 10x magnification (Nikon Eclipse TE2000-U with ACT-1 imaging software). Data for each treatment group were then merged and analyzed statistically. Concentration response curves were plotted for lethality from which LC_{50} values were calculated for 24 hpf. The experiments were performed in triplicate.

3. Results and discussion

3.1 Synthesis and spectroscopic characterization

Air and light stable crystalline $Ph_3PAu[SC(OR) = NC_6H_5]$, R = Me (**1**), Et (**2**), and iPr (**3**), were prepared in high yields as described previously [22] and following well established protocols [23], i.e., via the reaction of Ph_3PAuCl with the respective ROC(=S)N(H)Ph ligand [24] in the presence of base, and exhibited the same spectroscopic (^1H, $^{13}C\{^1H\}$ and $^{31}P\{^1H\}$

NMR and IR) characteristics [22]. Absorption spectra recorded in acetonitrile for **1**–**3** were virtually identical presenting three bands (Table S1). The most intense absorption was a high energy band centered at 240 nm which are assigned to inter-ligand π–π* transitions [25]. Two additional low energy bands with reduced intensity were observed at 267 and 275 nm. The low energy band involves transitions from the phosphane to the thiolate ligand. The remaining band appears to arise from transitions between the thiolate ligand and a delocalized state involving the entire molecule. Photoluminescence characteristics of **1**–**3** were also investigated by exciting each sample at the three absorption maxima discussed above. Two primary emission bands were observed with several weak shoulders (Table S2). Bands were of maximum intensity when λ_{ex} was 240 nm with the high energy bands (420-422 nm) being less intense than the low energy bands (486-489 nm). The relative intensities were inverted when λ_{ex} was 267 and 275 nm.

3.2 Mitochondrial cytochrome c measurements

The mitochondrial dependent cell death pathway contributes to the intrinsic pathway of apoptosis, a pathway that involves caspase-9. Upon induction of apoptosis by **1**–**3**, reactive oxygen species (ROS) will depolarize the mitochondrial membrane potential. This leads to the release of cytochrome c and pro-apoptotic proteins such as pro-caspase 9 from the intermembrane spaces of mitochondria into the cytosol leading to an intrinsic pathway of cell death. When released, cytochrome c will act with the pro-caspase 9 and apoptotic protease activating factor-1 (APAF-1) to activate the caspase cascade which promotes cell death [26]. Hence, the quantification of cytochrome c release from mitochondria of apoptotic cells can be used as an indicator of an apoptotic pathway.

The initial study on **1**–**3** [22] revealed significant expression of Bax while Bcl-2 expression decreased. This suggests in **1**–**3**-induced imbalance of the Bax/Bcl-2 ratio followed

by dysregulation of the mitochondrial membrane potential, and the subsequent activation of caspase-3 which may lead to irreversible apoptosis [22]. In addition, APAF-1 was also significantly upregulated by **1**–**3**. This result is consistent with cytochrome c binding to APAF-1 and procaspase-9 to form the apoptosome which activates the inactive procaspase-9 [22]. To confirm this mechanism, the cytosolic levels of cytochrome c after 6, 12 and 24 h exposure were analyzed, i.e., when caspase activity was at its maximum.

The untreated cells (negative control) showed low level release of cytochrome c from the mitochondria of HT-29 cells as seen in the concentration of the fluorescence population at M2 in the histograms shown in Fig. 2a. Less than 6 % of cytochrome c was released into the cytoplasm after 24 h. By contrast, the treated groups showed release of cytochrome c after as early as 6 h incubation as seen in the shift of the fluorescence population to M1 which arises as a result of binding by fluorescent anti-cytochrome c-FITC, Figs. 2b-d. After 24 h treatment of **1**–**3** about 97-99% of cytochrome c was released.

3.3 Flow cytometry for cell apoptosis analysis

An early event in apoptosis is loss of plasma membrane asymmetry which results in the exposure of phosphatidylserine (PS) residues at the outer plasma membrane leaflet [27]. As annexin V interacts strongly and specifically with PS, the measurement of annexin V can be employed to monitor apoptosis. In the untreated (negative control) samples, the majority of cells (99.61 %) were viable and non-apoptotic, Fig. 3a and Table 1, at 6 and 24 h. Non-apoptotic cells were marked as (Annexin V^-PI^-) as they remain the intact cell membrane. When cells were treated with IC_{50} concentrations of **1**–**3** for 6 h, the percentage of (Annexin V^-PI^-) dropped to 86~87 % and further reduced to 58~61 % when the incubation time reached 24 h. At 24 h, there was a significant increase in the population of early apoptotic cells with (Annexin V^+PI^-), i.e., increasing from ~0.32 % to ~25 %, Figs. 3b-d and Table 1. A slight increase in the

middle apoptosis stage, (Annexin V^+PI^+), was observed, indicating apoptosis proceeded with incubation time. The cells that died by necrosis, < 15 % at 24 h, were marked with (Annexin V^-PI^+).

3.4 Cell cycle analysis

Cell cycle and control of apoptosis are the significant regulatory mechanisms of cell growth, development, and differentiation. Cell cycle checkpoints guarantee the maintenance of genomic integrity by preventing DNA damage and incomplete DNA cells from further cell division. To further confirm the nature of apoptosis induced by **1**–**3**, the cell cycle distribution was determined at various times (6, 12 and 24 h) after exposure to the corresponding IC_{50} values.

As shown in Fig. 4 and Table 2, the population of untreated control cells at G_2/M after 24 h was 2.29%. After being treated with **1**–**3** the number of cell significantly increased at the G_2/M phase i.e., ca. 40 %. This was accompanied by a significant decrease in the G_1 phase cf. the untreated control cells, Table 2. The G_2/M checkpoint is operative in the late G_2 phase and allows for the repair of damaged DNA in the late S or G_2 phases, i.e., before proceeding to the mitosis (M) stage. Hence, the G_2 checkpoint functions to prevent damaged DNA being segregated into daughter cells. At this checkpoint, cdc2 (CDK1) forms a complex with cyclin B1 (CCNB1). The resulting cdc2-cyclin B1 complex plays a critical role in regulation of the G_2/M phase and its inactivation inhibits the transition from the G_2 to M phase [28]. The cdc2 and cyclin B1 genes have been significantly downregulated by **1**–**3**, Fig. 5. In addition, the M phase inducer, phosphatase 3 (cdc25C), which plays an important role in the dephosphorylation of cdc2 leading to the activation of the cyclin B1/cdc2 complex [29], is also downregulated by **1**–**3**. Moreover, phosphorylation of cdc25C on serine-216 by Chk1 or Chk2 generates a binding site for 14-3-3 proteins and results in the dissemination of phosphorylated cdc25C to

the cytoplasm and its retention there. In the present study upon treatment with **1**–**3**, Chk1 was upregulated from 12 h to 24 h by 1.81-, 2.33-, and 3.08-fold, respectively, so nuclear cdc2 remains phosphorylated in the absence of cdc25C and the cells remain arrested in the G_2 phase [30,31].

One of the important regulators of the cell cycle and a downstream target of p53 is CDKN1A, which encodes p21. The expression of p21 is induced by p53 [32,33]. p21 is a potent cyclin-dependent kinase inhibitor that binds to and then inhibits the activity of cyclin-CDK2 or -CDK4 complexes and thus functions as a negative regulator of cell cycle progression [33-35]. DNA damage or genotoxic stress induced by **1**–**3** activates ATR which then phosphorylates CHEK1 and probably p53 [36]. Upon phosphorylation, p53 is stabilized and activated, and subsequently induces the expression of $p21^{Waf/CIP}$ (CDKN1A) which inhibits CDK1-cyclin B1 activity, leading to G_2/M arrest [36]. Compounds **1**–**3** upregulated CDKN1A, by 2.99-, 1.98- and 1.81-fold from 12 to 24 h (Fig. 5). In the same way, the ATR gene was upregulated by 5.11-, 4.55-, and 5.71-fold, respectively, after 24 h.

Stimulation of p53 expression also leads to DNA damage and results in induction of GADD45 [37]. Interestingly, GADD45 destabilizes the cyclin B1/cdc2 complex *in vitro* suggesting that it may mediate cyclin B1/cdc2 complex inactivation *in vivo* [38]. GADD45 was significantly upregulated by **1**–**3**, i.e., 6.43-, 7.87- and 11.42-fold, respectively, compared to the control (Fig. 5).

3.5 Cell invasion study

The suppression or inhibition of cancer cell migration and invasion is a crucial target of chemotherapy [39], with the obvious aim to reduce the chances of cancer metastasis into secondary organs such as the brain, lung, and liver [40]. It is recognized that the attachment of β-Catenin onto the T-cell factor (Tcf) of DNA leads to expression of survivin (BIRC5) and

consequently enhanced cell metastasis and angiogenesis [41,42]. The metastasis rate of colorectal cancer is high compared with other cancers because colorectal cancer cells are most abundant in Tcf [41,42]. As shown in Fig. 5, BIRC5 was downregulated after the 24 h incubation period, i.e., -2.98-, -1.76-, and -1.32-fold, respectively for **1**–**3**.

A cell invasion assay was performed to investigate the activity of **1**–**3** toward inhibition of metastasis of HT-29 cancer cells. Matrigel^{TM} invasion chamber is an endothelial like model for the study of the prevention of cancer cell invasion. As illustrated in Fig. 6, **1**–**3** inhibited the invasion of HT-29 cells through Matrigel^{TM} with rates decreased to 17.71±0.89 %, 18.54±1.20 %, and 21.85±1.53 %, respectively compared with the negative control (normalized to 100%).

Based on research by Mehrotra et al. [43], the activation of the cell motility kinases focal adhesion kinase (FAK) and c-Src tyrosine kinase (c-Src) by NF-κB contributes to cancer progression and metastasis, and the activity of NF-κB is related to survivin [59]. Activation of survivin is due to the mutation of WnT signaling leading to further activation of β-Catenin. Activated NF-κB can selectively bind DNA and leads to irregular expression of genes related to apoptosis, promotes cell proliferation, releases proteins needed for angiogenesis, and stimulates invasion and metastasis [44,45]. Thus, evidence of downregulation of survivin by **1**–**3** [22] coupled with downregulation of XIAP expression, i.e., -7.28-, -3.44-, and -5.87-fold, respectively (Fig. 9), leads to the inhibition of metastasis in HT-29 cells.

Other inhibition effects on NF-κB were promoted by **1**–**3**. The inhibition of NF-κB leads to further inhibition of the synthesis of metalloproteineases, MMP2 and MMP9 which regulate tumor invasiveness [46]. According to Fig. 5, MMP2 was significantly downregulated by **1**–**3**, i.e., by 6.42-, 6.79- and 7.92-fold, respectively. The inhibition of metalloproteineases prevents the basement membrane of endothelial cells in blood vessels from degrading [47,48].

3.6 Related complexes

The new results complement the $Ph_3PAu[SC(OR) = N(p\text{-tolyl})]$, R = Me (**4**), Et (**5**) and iPr (**6**), series which was shown also to induce apoptosis by extrinsic and intrinsic pathways, and to downregulate NF-κB [49]. Further, **4** did not upregulate p53 or p73, **5** upregulated both whereas **6** only upregulated p53. This interdependence on R and the nature of the N-bound aryl group suggests compound specific biological activity. Over and above the anti-cancer potential of **4**–**6**, these have also proved to exhibit broad range antimicrobial activity against Gram positive bacteria, including against multidrug resistant strains of methicillin resistant *S. aureus* (MRSA), and to be bactericidal [50]. The foregoing suggests this class of compound is well worthy of further, systematic investigation for biological potential and may complement platinum drugs for the treatment of cancer [51].

3.7 Zebrafish embryo toxicity

The zebrafish embryo is a useful research model to study human disease, nanoparticle toxicity, and drug screening because it is small, transparent, undergoes rapid embryo genesis, the fish continuously reproduce, and are easy to maintain [52]. Over and above these considerations, zebrafish embryos have a high degree of homology to the human genome, which ensures this living organism is useful for toxicological studies [52,53]. Representative images of zebrafish embryos treated with **1**–**3** at concentrations 0.625, 1.25, 2.5, and 5.0 μM are shown in Fig. 7. The negative control (1 % DMSO) did not show mortality and morphological changes were as shown in Fig. 7 (top). The percentage survival decreased with increasing concentrations of **1**–**3** as shown in Fig. 8.

The changes in the morphology of zebrafish embryos were monitored using a stereomicroscope during the first 72 h of exposure. The difference in total length of larvae exposed to various concentrations of **1**–**3** was found to be insignificant. In the control groups,

no deformities were detected. All embryos and larvae showed wild-type phenotype and developed normally having normal eyes, pigmentation, straight trunk and tail, and no edema at 0.625 µM of **1**–**3** (Fig. 7). When the concentration of **1** and **2** was 1.25 µM (Fig. 7a, b), the following observations were made: the tail length of the larvae reduced in size and tended to bend and the body shape was also bent. Further, slight edema and egg yolk extension deformation or pericardial edema were evident. More encouraging was the observation that overall body shape, heart, and pericardial sac of the larvae were normal after treatment with **3** at the same concentration (Fig. 7c), indicating **3** is less toxic in this model at 1.25 µM. Finally, the LC_{50} at 24 hpf for **3** is 7.64 µM, lower than **1** and **2** where LC_{50} are 8.36 and 8.17, respectively. When the concentration of **1**–**3** was increased from 1.25 to 5.0 µM, both poor pigmentation and morphological disorder were observed (Fig. 7). At higher concentrations, the compounds were lethal.

Conclusions

Further physiochemical and biological investigations have been conducted on phosphanegold thiolates, $Ph_3PAu[SC(OR) = NPh]$, R = Me (**1**), Et (**2**) and iPr (**3**) which display cytotoxicity toward HT-29 cancer cells and to induce cell death by both intrinsic and extrinsic apoptotic pathways [22]. Mitochondrial cytochrome c measurements confirmed apoptotic pathways of cell death supported by PCR (upregulation of APAF-1). The anti-cancer effect was associated with the capacity of **1**–**3** to trigger growth inhibition at the G_2/M phase at 12 and 24 h through the downregulation of cdc2, cdc25C and cyclin B1 and the upregulation of p21. Cell invasion studies showed inhibition of metathesis through Matrigel™ matrix to 17-22 % cf. untreated cells. LC_{50} values were determined in zebrafish to be 8.36, 8.17, and 7.64 µM for **1**–**3**, respectively. The zebrafish tolerated doses of **1**–**3** up to 0.625 µM; **3** was tolerated at even higher doses up to 1.25 µM.

Acknowledgements

Sunway University and The Ministry of Higher Education (Malaysia) is thanked for funding (UM.C/HIR-MOHE/SC/12).

Appendix A. Supplementary data

Supplementary data to this article can be found online at http://

References

[1] S.J. Berners-Price, P.J. Sadler, Struct Bond (Berlin) 70 (1988) 27–102.

[2] E.R.T. Tiekink, Crit. Rev. Hematol. Oncol. 42 (2002) 225–245.

[3] C.F. Shaw, Chem. Rev. 99 (1999) 2589–2600.

[4] P.J. Barnard, S.J. Berners-Price, Coord. Chem. Rev. 251 (2007) 1889–1902.

[5] I. Ott, Coord. Chem. Rev. 253 (2009) 1670–1681.

[6] S.J. Berners-Price, A. Filipovska, Metallomics, 3 (2011) 863–873.

[7] B. Bertrand, A. Casini, Dalton Trans. 43 (2014) 4209–4219.

[8] T. Zou, C.T. Lum, C.-N. Lok, J.-J. Zhang, C.-M. Che, Chem. Soc. Rev. 44 (2015) 8786–8801.

[9] D.R. Green, G. Kroemer, Science 305 (2004) 626–629.

[10] S.J. Ralph, S. Rodríguez-Enríquez, J. Neuzil, E. Saavedra, R. Moreno-Sánchez, Mol. Aspects Med. 31 (2010) 145–170.

[11] S.P. Jackson, J. Bartek, Nature 461 (2009) 1071–1078.

[12] A.W. Murray, Cell 116 (2004) 221–234.

[13] K. Collins, T. Jacks, N.P. Pavletich, Proc. Natl Acad.Sci. USA 94 (1997) 2776–2778.

[14] A. Karimian, Y. Ahmadi, B. Yousefi, DNA Repair 42 (2016) 63–71.

[15] W.L. Seng, K. Eng, J. Lee, P. McGrath, Angiogenesis 7 (2004) 243–253.

[16] C.A. Staton, W.R. Malcolm, N.J. Brown, Int. J. Exp. Pathol. 90 (2009) 195–221.

[17] A. Letamendia, C. Quevedo, I. Ibarbia, J.M. Virto, O Holgado, M. Diez, J.C. Izpisua-Belmonte, C. Callol-Massot, PLoS One 7 (2012) e36690.

[18] M. Westerfield, The zebrafish book. A guide for the laboratory use of zebrafish (Danio rerio). 5th ed., University of Oregon Press, Eugene (2007).

[19] K. Howe, M.D. Clark, C.F. Torroja, J. Torrance, Nature 496 (2013) 498–503.

[20] A.J. Hill, H. Teraoka, W. Heideman, R.E. Peterson, Toxicol. Sci. 86 (2005) 6–19.

[21] S.S. Dhillon, E. Dóró, I. Magyary, S. Egginton, A. Sík, F. Müller, PloS One 8 (2013) e60552

[22] C.I. Yeo, K.K. Ooi, A.Md Akim, K.P. Ang, Z.A. Fairuz, S.N.Bt.A. Halim, S.W. Ng, H.-L. Seng, E.R.T. Tiekink, J. Inorg. Biochem. 127 (2013) 24–38.

[23] V.J. Hall, G. Siasios, E.R.T. Tiekink, Aust. J. Chem. 46 (1993) 561–570.

[24] S.Y. Ho, R.P.A. Bettens, D. Dakternieks, A. Duthie, E.R.T. Tiekink, CrystEngComm 7 (2005) 682–689.

[25] S.Y. Ho, E.C.-C. Cheng, E.R.T. Tiekink, V.W.-W. Yam, Inorg. Chem. 45 (2006) 8165–8174.

[26] I. Zlobec, P. Minoo, K. Baker, D. Haegert, K. Khetani, L. Tornillo, L. Terracciano, J. R. Jass, A. Lugli, Eur. J. Cancer 43 (2007) 1101–1107.

[27] E.A. Nigg, Cell. Develop. Biol. 17 (1995) 471–480.

[28] S.J. Park, S. W. Yang, B.C. Kim, Biochem. Biophys. Res. Commun. 472 (2016) 502–507.

[29] P. Jin, Y. Gu, D.O. Morgan, J. Cell Biol. 134 (1996) 963–970.

[30] A. Lopez-Girona, B. Furnari, O. Mondesert, P. Russell, Nature 397 (1999) 172–175.

[31] C.Y. Peng, P.R. Graves, R.S. Thoma, Z. Wu, A.S. Shaw, H. Piwnica-Worms, Science 277 (1997) 1501–1505.

[32] P.P. McKenzie, S.M. Guichard, D.S. Middlemas, R.A. Ashmun, M.K. Danks, L.C. Harris, Clin. Cancer Res. 5 (1999) 4199–4207.

[33] F. Bunz, A. Dutriaux, C. Lengauer, T. Waldman, S. Zhou, J.P. Brown, J.M. Sedivy, K.W. Kinzler, B. Vogelstein, Science 282 (1998) 1497–1501.

[34] J.W. Harper, G.R. Adami, N. Wei, K. Keyomarsi, S.J. Elledge, S. J. Cell 75 (1993) 805–816.

[35] T. Waldman, K.W. Kinzler, B. Vogelstein, B. Cancer Res. 55 (1995) 5187–5190.

[36] J.-J. Rong, R. Hu, X.-M. Song, J. Ha, N. Lu, Q. Qi, L. Tao, Q.-D. You, Q.-L. Guo, Cancer Lett. 296 (2010) 55–64.

[37] E. Matsunaga, S. Nambu, M. Oka, A. Iriki, Neuroscience 284 (2015) 566–580.

[38] Q. Zhan, M.J. Antinore, X.W. Wang, F. Carrier, M.L. Smith, C.C. Harris A.J. Fornace Jr., Oncogene 18 (1999) 2892–2900.

[39] J.C. Cheng, C.H. Chou, M.L. Kuo, C.Y. Hsieh, Oncogene 25 (2006) 7009–7018.

[40] B.B. Ma, E.P. Hui, A.T. Chan, Cancer Science 99 (2008) 1311–1318.

[41] S. Angers, R.T. Moon, Nat. Rev. Mol. Cell Biol. 10 (2009) 468–477.

[42] B.T. MacDonald, K. Tamai, X. He, Dev. Cell 17 (2009) 9–26.

[43] S. Mehrotra, L.R. Languino, C.M. Raskett, A.M. Mercurio, T. Dohi, D.C. Altieri, Cancer Cell 17 (2010) 53–64.

[44] B.K. Park, H. Zhang, Q. Zeng, J. Dai, E.T. Keller, T. Giordano, Nat. Med. 13 (2007) 62–69.

[45] Y. Wu, J. Deng, P.G. Rychahou, S. Qiu, B.M. Evers, B.P. Zhou, Cancer Cell 15 (2009) 416–428.

[46] C.T. Yeh, Y.K. Rao, M. Ye, W.S. Wu, T.C. Chang, L.S. Wang, C.H. Wu, T.H. Alexander Wu, Y.W. Tzeng, Toxicol. Appl. Pharmacol. 261 (2012) 31–41.

[47] F.G. Giancotti, E. Ruoslathi, Science 285 (1999) 1028–1032.

[48] Z.S. Zeng, A.M. Cohen, J.G. Guillem, Carcinogenesis 20 (1999) 749–755.

[49] K.K. Ooi, C.I. Yeo, K.-P. Ang, A.Md. Akim, Y.-K. Cheah, S.N.A. Halim, H.-L. Seng, E.R.T. Tiekink, J. Biol. Inorg. Chem. 20 (2015) 855–873.

[50] C.I. Yeo, J.-H. Sim, C.-H. Khoo, Z.-J. Goh, K.-P. Ang, Y.-K. Cheah, Z.A. Fairuz, S.N.B.A. Halim, S.W. Ng, H.-L. Seng, E.R.T. Tiekink, Gold Bull. 46 (2013) 145–152.

[51] C.S. Allardyce, P.J. Dyson, Dalton Trans. 45 (2016) 3201–3209.

[52] P.V. Asharani, Y. Lianwu, Z. Gong, S. Valiyaveettil, Nanotoxicology 5 (2011) 43–54.

[53] J.P. Berry, M. Gantar, P.D.L. Gibbs, M.C. Schmale, Comp. Biochem. Physiol., Part C: Toxicol. Pharmacol. 145 (2007) 61–72.

Table 1

Summary of cell populations in the quadrant graphs of Fig. 3.[a]

	Negative Control (%)		**1** (%)		**2** (%)		**3** (%)	
	6h	24h	6h	24h	6h	24h	6h	24h
L	99.63	99.61	86.27	58.05	86.35	61.25	87.09	58.77
EA	0.26	0.32	3.61	25.54	8.35	25.24	8.94	24.63
MA	0.10	0.05	2.25	2.02	2.36	1.08	1.84	2.34
N	0.01	0.02	7.88	14.39	2.93	12.42	2.13	14.26

a The proportion of annexin V stained cells increased with increasing incubation time. L = non apoptotic cell, EA = early apoptosis, MA = middle apoptosis, and N = necrosis.

Table 2

Summary of cell cycle distribution (%) in the graphs of Fig. 4.

	Negative control			**1**			**2**			**3**		
	6h	12h	24h	6h	12h	24h	6h	12h	24h	6h	12h	24h
G_0/G_1	94.27	94.36	94.20	65.43	59.50	40.10	69.50	52.65	37.68	67.43	59.68	41.60
S	3.61	3.57	3.60	11.80	19.98	17.10	11.22	19.80	17.81	12.98	17.48	13.94
G_2/M	2.22	2.17	2.29	21.46	23.20	40.25	18.82	27.23	39.73	18.87	21.40	43.37
Sub G_0	0.30	0.35	0.27	0.20	0.46	2.08	0.20	0.24	4.26	0.10	0.55	1.06

Captions to Schemes/Figures

Fig. 1. Chemical structures of the triphenylphosphanegold(I) carbonimidothioates (**1**–**3**) investigated herein.

Fig. 2. Histograms representing the cells stained using the FlowCellet cytochrome c kit™ after 6, 12, and 24 h: (a) Untreated group (negative control) of HT-29 cells, (b) HT-29 cells treated with 11.30 µM of **1**, (c) 17.00 µM of **2**, and (d) 16.80 µM of **3**. Histograms in b-d show downward shifts (from M2 to M1) in fluorescence levels due to cytochrome c.

Fig. 3. Quadrant graphs of cell apoptosis analysis after 6 and 24 h incubation time. Note there is an increasing percentage of cells undergoing apoptosis as the incubation time increases, and eventually they will become necrotic. (a) Untreated cells (negative control), (b) treated with 11.30 µM of **1**, (c) 17.00 µM of **2**, (d) 16.80 µM of **3**.

Fig. 4. Effect on cell cycle distribution in HT-29 cells. Cells were incubated at the respective IC_{50} doses (b) **1** [11.30 µM], (c) **2** [17.20 µM], and (d) **3** [16.80 µM], with (a) being the untreated group [negative control]. Cells were incubated for 6, 12, and 24 h, and the distribution of cell cycle was determined by the FACS Calibur method.

Fig. 5. Cell cycle gene expression level in HT-29 cell lines at 12 and 24 h compared to untreated cells (corresponding to value 1) after treatment with (a) **1** [11.30 µM], (b) **2** [17.20 µM], and (c) **3** [16.80 µM] at the respective IC_{50} doses. *$p < 0.05$.

Fig. 6. Matrigel™ invasion assay showing **1**–**3** inhibited cell invasion. (a) Photos were taken at 200x magnification, and are representative of three independent experiments. (b) Graphical representation of the numbers of invaded cells per microscopic fields when treated with **1**–**3**. Data were shown as mean ± SEM from three independent experiments. *$p < 0.05$, compared to the 1 % DMSO only. The invasion rates of **1**–**3** are 17.71 ± 0.89%, 18.54 ± 1.20%, and 21.85 ± 1.53%, respectively (normalized to 100%).

Fig. 7. Morphological analysis of negative control (1 % DMSO) and toxicity of (a) **1**, (b) **2**, and (c) **3** at 0.625-5.0 μM at 3dpf.

Fig. 8. Graph representing the toxicity of **1**–**3** in terms of survival rate of larvae at 3dpf. Data represents mean ± SD (n = 40).

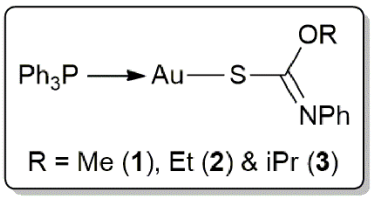

Figure 1

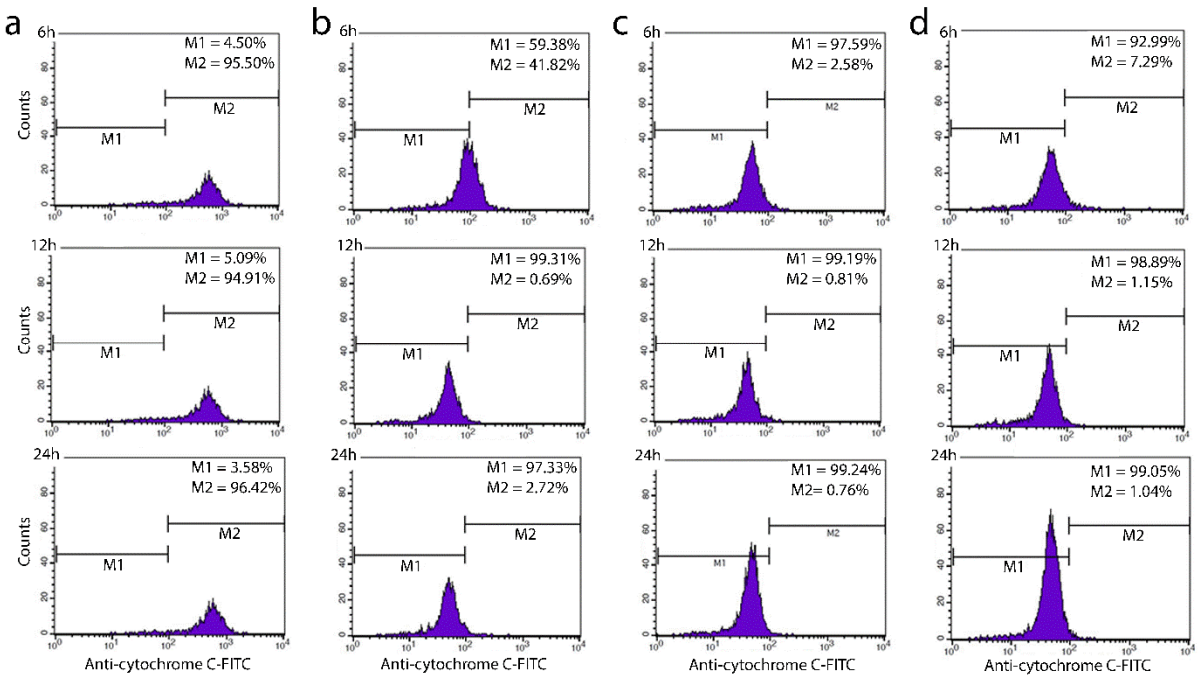

Figure 2

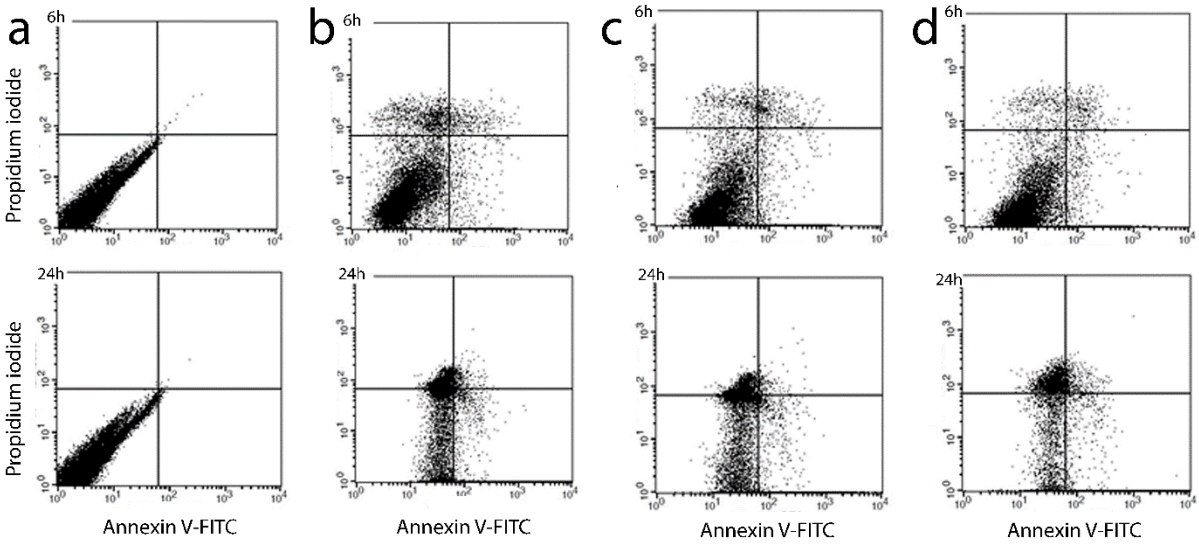

Figure 3

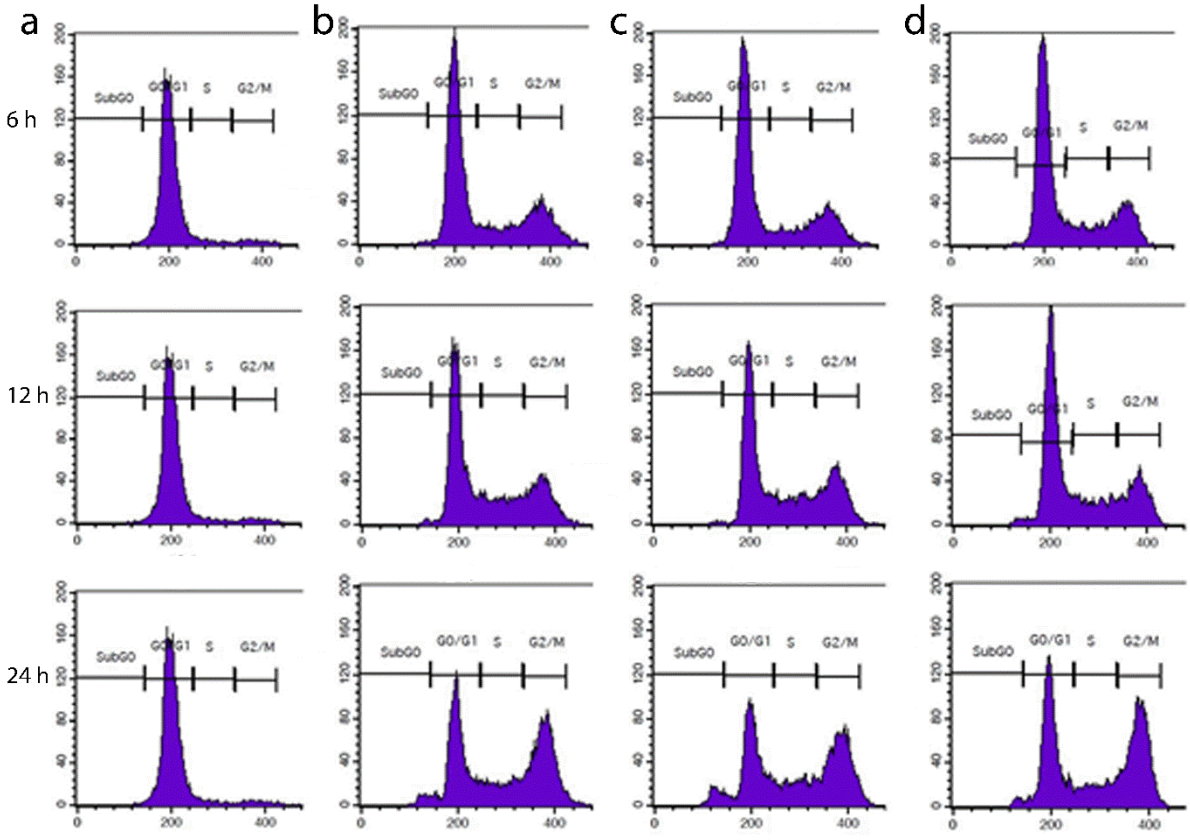

Figure 4

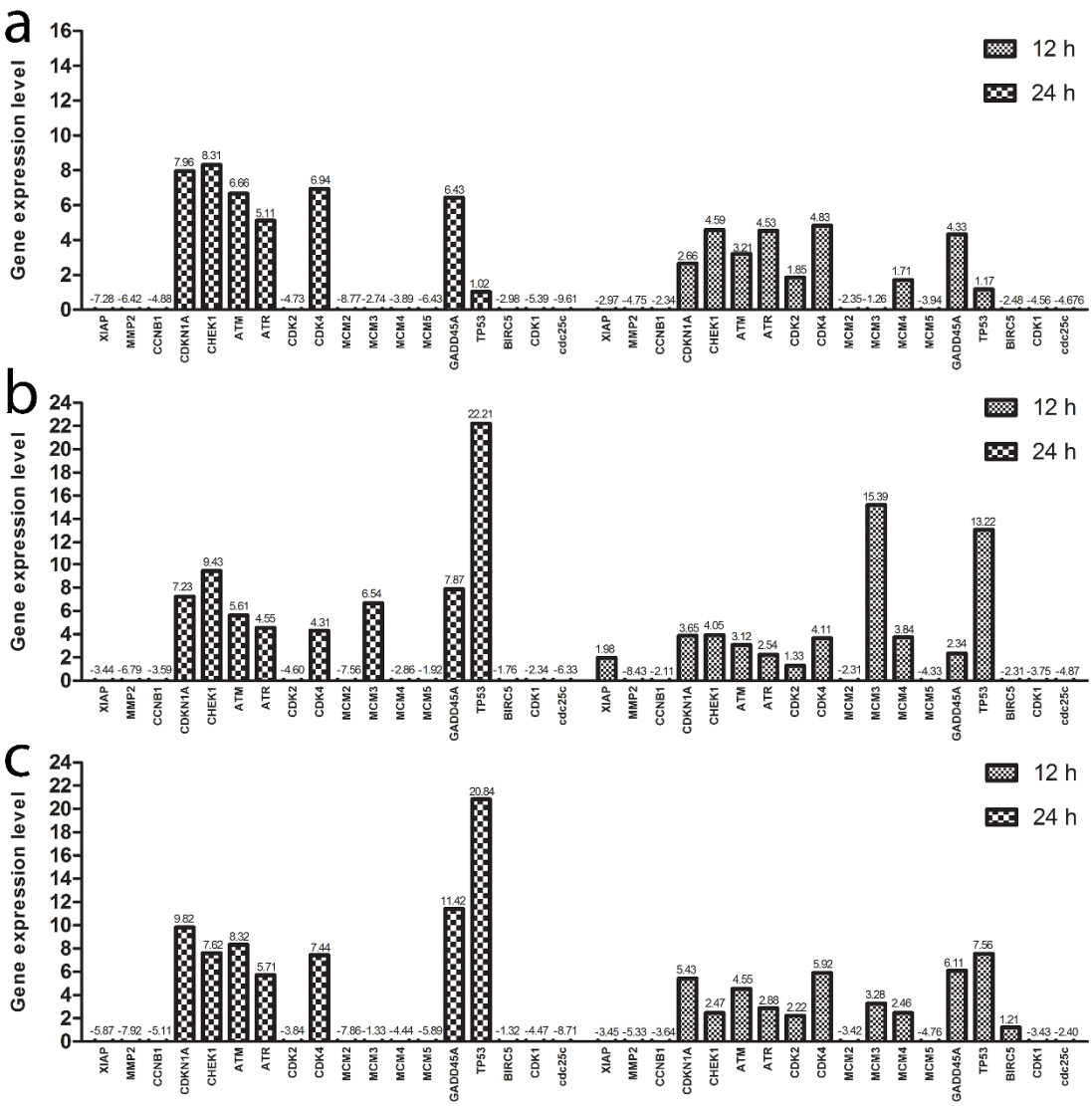
a
b
c
Gene expression level
12 h
24 h
XIAP
MMP2
CCNB1
CDKN1A
CHEK1
ATM
ATR
CDK2
CDK4
MCM2
MCM3
MCM4
MCM5
GADD45A
TP53
BIRC5
CDK1
cdc25c

Figure 5

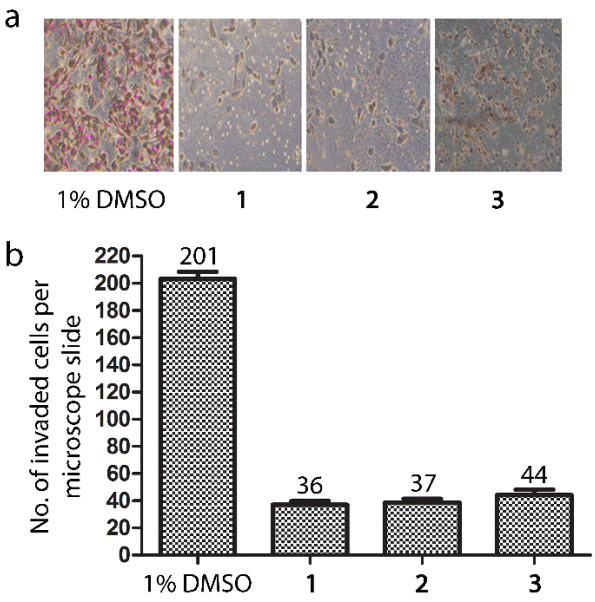

Figure 6

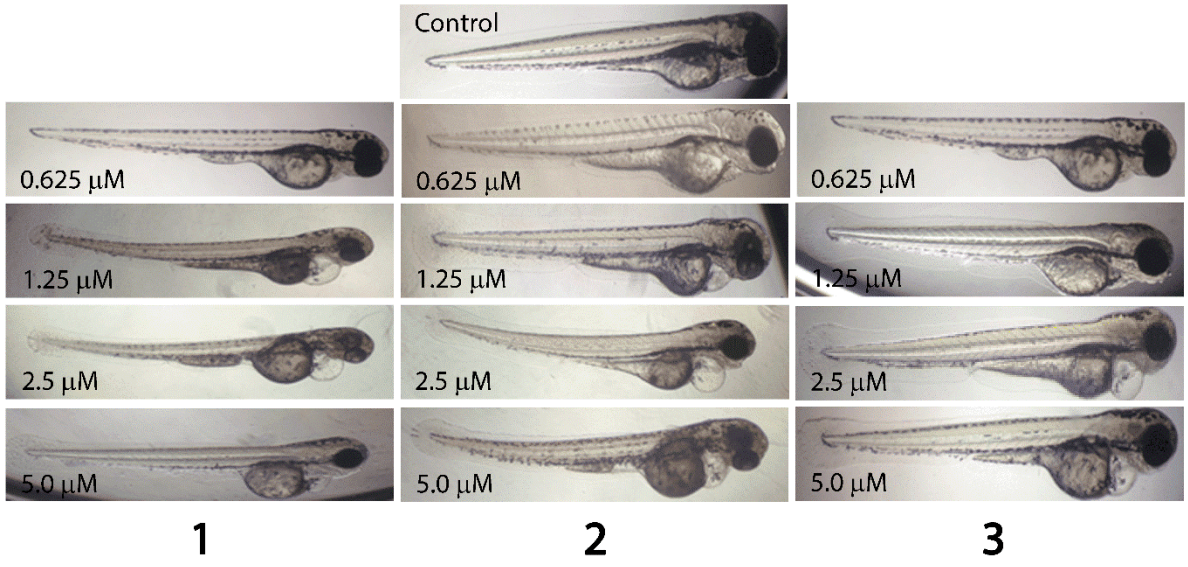

Figure 7

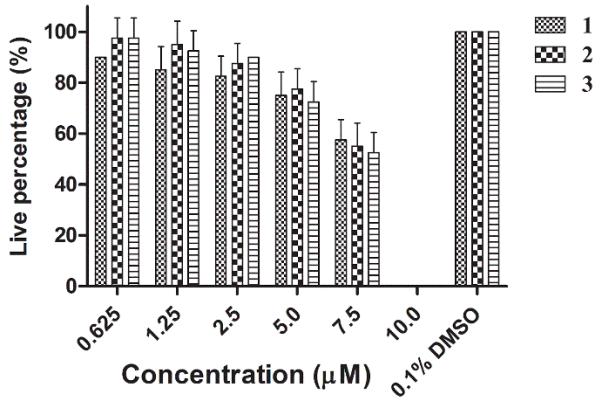
Live percentage (%)
100
80
60
40
20
0
0.625
1.25
2.5
5.0
7.5
10.0
0.1% DMSO
Concentration (μM)
1
2
3

Figure 8